Chinese Chemical Letters 37 (2026) 111284

Contents lists available at ScienceDirect

Chinese Chemical Letters

journal homepage: www.elsevier.com/locate/cclet

Orthogonal upconversion nanoplatform for *in situ* hydrogelation and photo-activatable chemotherapy

Minfei Yu[a], Yueyan Yang[a], Xin Cheng[a], Shicheng Pei[a], Man Wu[a], Fangling Cao[a], Yaxin Zheng[a], Shuyao Zhou[a], Keming Xu[a,b,*], Lei Zhou[a,b,*], Wenying Zhong[a,b,*]

[a] School of Science, China Pharmaceutical University, Nanjing 211198, China
[b] Key Laboratory of Biomedical Functional Materials, China Pharmaceutical University, Nanjing 211198, China

ARTICLE INFO

Article history:
Received 1 March 2025
Revised 27 April 2025
Accepted 30 April 2025
Available online 30 April 2025

Keywords:
Upconversion nanoparticles
Light-responsive
Photopolymerization hydrogel
Prodrug activation
Spatiotemporal drug delivery

ABSTRACT

Light is a powerful tool for controlling hydrogel formation and drug release, which are essential in tissue engineering and drug delivery. Achieving orthogonal control over hydrogelation and drug release using different wavelengths of light offers precise spatiotemporal regulation but is challenged by limited penetration depth and spectral crosstalk of commonly used visible light. Herein, this work develops an orthogonal light-responsive hydrogel based on dual-wavelength upconversion nanoparticles (UCNPs) for controlled hydrogelation and drug release. Upon 808 nm excitation, these UCNPs emit green light, triggering the photopolymerization of hyaluronic acid-2-aminoethyl methacrylate hydrogels. While 980 nm induces ultraviolet emission, enabling controlled and sustained drug release. Through structural design, the emissions under dual-wavelength excitation exhibit no spectral crosstalk, enabling orthogonal light control of both processes. *In vitro* and *in vivo* experiments show that both hydrogel formation and drug release processes can be finely tuned by controlling the power density and excitation durations, significantly enhancing the spatiotemporal precision of drug delivery. This orthogonal light-responsive hydrogel holds significant potential for precise, spatiotemporally controlled drug delivery.

© 2026 Published by Elsevier B.V. on behalf of Chinese Chemical Society and Institute of Materia Medica, Chinese Academy of Medical Sciences.

Hydrogel has emerged as a versatile platform in drug delivery [1–3], offering substantial promise for targeted therapies in oncology. Among the reported hydrogels, stimulus-responsive hydrogels are particularly important due to their ability to mitigate the systemic side effects typically associated with chemotherapy. These hydrogels respond to specific physiological stimuli such as enzymes [4,5], temperature [6–8], or pH [9–11], enabling site-specific drug release. However, the clinical translation of these hydrogels faces challenges, including uncontrolled mechanical strength and immature drug release.

Recently, light-responsive hydrogel has gained great interest for its potential in precise drug delivery [12–19]. It employs light as a trigger for prodrug cleavage and subsequent drug release, facilitating on-demand therapy. Besides that, light can initiate photopolymerization [20–22], allowing for the customization of hydrogel's physical and chemical properties. We envision that achieving orthogonal control over both hydrogel mechanical strength and drug release within a single system could enable long-term, precise drug delivery; however, the simultaneous achievement of both functions still remains a challenge. The main obstacle is the limited penetration depth of conventional light sources [23,24], such as ultraviolet (UV) [25,26] and visible light [15,27], used in current light-responsive hydrogels. While these wavelengths have sufficient photon energy to activate light- responsive reactions, they suffer from poor tissue penetration and are prone to spectral overlap, causing unintended crosstalk between hydrogelation and drug release. This significantly limits their effectiveness for targeting deep-seated tumors. Therefore, it is highly desired to develop light-responsive hydrogels that operate with high penetration light and allow orthogonal control of hydrogelation and drug release.

A breakthrough in addressing these challenges comes from the development of upconversion nanoparticles (UCNPs) [28–34]. These nanoparticles convert deeply-penetrating near-infrared (NIR) light into visible or UV light, effectively triggering a variety of light-responsive processes [35]. Furthermore, UCNPs can be engineered to exhibit orthogonal luminescence, emitting different wavelengths of light in response to varying NIR excitations [36,37]. This unique feature allows for the creation of orthogonal hydrogel systems that combine precise *in-situ* hydrogelation and light-controlled prodrug activation. However, a light-responsive hydrogel

* Corresponding authors.
E-mail addresses: kmxu@cpu.edu.cn (K. Xu), leizhou@cpu.edu.cn (L. Zhou), wyzhong@cpu.edu.cn (W. Zhong).

https://doi.org/10.1016/j.cclet.2025.111284
1001-8417/© 2026 Published by Elsevier B.V. on behalf of Chinese Chemical Society and Institute of Materia Medica, Chinese Academy of Medical Sciences.

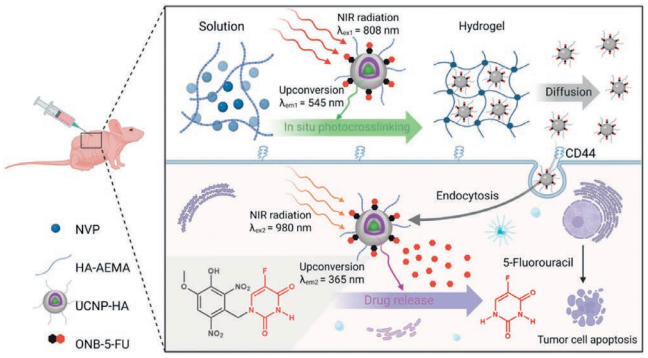


Fig. 1. Schematic illustration of photopolymerized hydrogelation and *in vivo* drug release by a dual-wavelength orthogonal UCNP-based nanoplatform.

system with dual-wavelength orthogonal NIR activation has not yet been reported.

Herein, we present a dual-wavelength orthogonal UCNPs-based nanoplatform system that allows for precise control over both NIR-responsive hydrogel photopolymerization and prodrug activation followed by the release of 5-fluorouracil (5-FU), enabling enhanced tissue penetration and targeted cancer therapy (Fig. 1). Our system features a multi-layered UCNPs design (β-$NaGdF_4$:Yb20 %/Er2 %@$NaYF_4$:Yb20 %@$NaGdF_4$:Yb20 %/Nd50 %@$NaYF_4$@$NaGdF_4$:Yb80 %/Tm1 %@$NaYF_4$), optimized to harness the energy from 808 nm to 980 nm excitations, upconvert to 545 nm and 365 nm for the *in-situ* photopolymerized hydrogelation and prodrug activation, respectively. After incorporating UCNPs into a hyaluronic acid-2-aminoethyl methacrylate (HA-AEMA) hydrogel, 808 nm irradiation initiates photopolymerization, forming a matrix that acts as a reservoir for both prodrugs and UCNPs. The HA-modified UCNPs bind to the CD44 receptor on tumor cells, facilitating cellular accumulation [38]. Subsequent 980 nm irradiation activates ONB-5-FU, leading to cell death. Our findings underscore the efficiency of this platform in achieving rapid hydrogelation within five minutes and allowing adjustable crosslinking densities based on 808 nm irradiation times. The subsequent 980 nm excitation led to a significant cytotoxic effect against B16-F10 melanoma cells. Furthermore, *in vivo* studies demonstrated the potential of this approach for targeted cancer therapy, as evidenced by the effective inhibition of tumor growth in a B16-F10-xenografted mouse model, without notable systemic toxicity. To the best of our knowledge, this is the first instance that combines dual-wavelength orthogonal UCNPs for hydrogel photopolymerization and drug activation with targeted delivery. We believe that the dual-wavelength orthogonal NIR light-responsive hydrogel system will be an effective nanoplatform for more accurate and less harmful cancer treatments.

The multilayer core-shell nanostructure β-$NaGdF_4$:Yb20 %/Er2 %@$NaYF_4$:Yb20 %@$NaGdF_4$:Yb20 %/Nd50 %@$NaYF_4$@$NaGdF_4$:Yb80 %/Tm1 %@$NaYF_4$ UCNPs were designed to achieve dual emissions through precise control of excitation energy orientation (Fig. 2). The multilayer core-shell structure was segmented by $NaYF_4$ inert layers into two parts, each conducting an independent upconversion process to yield dual emissions: green emission at ~545 nm with 808 nm excitation, UV emission at ~365 nm with 980 nm excitation (Fig. 2D). The synthesized UCNPs were characterized using transmission electron microscopy (TEM). Fig. 2A shows the alternating bright and dark layers of these UCNPs, which can be explained by the contrast difference between gadolinium (Gd, $Z = 64$) and yttrium (Y, $Z = 39$) in different layers, indicating successful shell growth. Energy dispersive X-ray spectroscopy (EDX) mapping of a single nanocrystal successfully confirmed the presence of all expected elements (Fig. S1 in Supporting information). The UCNPs showed an average diameter of ~60 nm and a uniform size distribution (Fig. 2B), which is consistent with the dynamic light scattering (DLS) measurements (Table S1 in Supporting information). The upconversion emission spectra and the related emission mechanisms are displayed in Figs. 2C and D. Upon 808 nm excitation, Nd^{3+} undergoes excitation ($^4I_{9/2} \rightarrow {}^4F_{5/2}$) and transfers energy to Yb^{3+}($^2F_{7/2} \rightarrow {}^2F_{5/2}$), subsequently transferring the energy to Er^{3+} located within the core ($^4S_{3/2} \rightarrow {}^4I_{15/2}$), resulting in the upconversion emission at approximately 545 nm. Tm^{3+} in the outer shell is excited by the 980 nm NIR laser with Yb^{3+}acting as a sensitizer ($^2F_{7/2} \rightarrow {}^2F_{5/2}$), leading to the emission of blue and UV light at around 450 nm ($^1D_2 \rightarrow {}^3F_4$) and 365 nm ($^1D_2 \rightarrow {}^3H_6$), respectively. The presence of Y^{3+} in the middle and outermost shells plays a crucial role in preventing cross-relaxation and surface quenching, thereby augmenting the efficiency of upconversion luminescence.

The hydrogel was composed of UCNPs, HA-AEMA, Eosin Y, triethanolamine (TEOA) and *N*-vinylpyrrolidone (NVP). UCNPs prepared above were utilized to *in-situ* convert the 808 nm light to green light, aiding the photopolymerization process. Eosin Y, activated by 545 nm green light, served as the photo-initiator, while TEOA acted as co-initiator. NVP, a co-monomer, was copolymerized with HA-AEMA to enhance the hydrogel's crosslinking speed and mechanical strength. The HA-AEMA was synthesized *via* an 1-ethyl-3-(3-dimethylaminopropyl)carbodiimide/*N*-hydroxysuccinimide (EDC/NHS) reaction (Figs. S2 and S3 in Supporting information). After optimization (Table S2 in Supporting information), the final hydrogel composition, referred to as formula

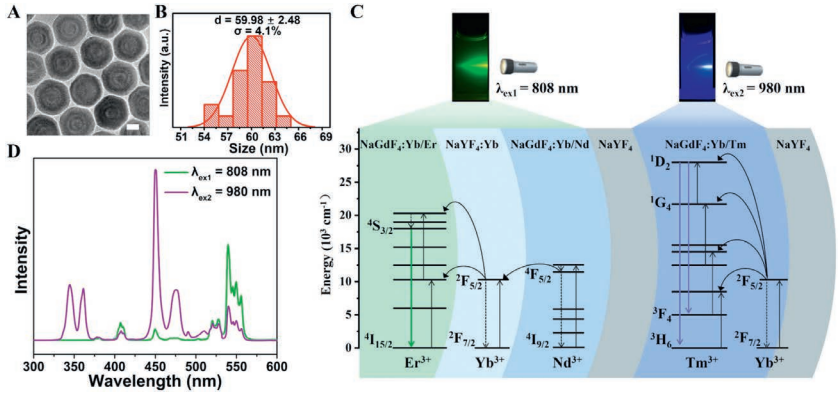


Fig. 2. Characterization of dual-wavelength orthogonal UCNPs. (A) TEM image and (B) size distribution of UCNPs. (C) Schematic illustration of energy transfer upconversion processes in UCNPs. (D) Upconversion emission spectra excited by 808 and 980 nm laser, respectively. Scale bar: 20 nm.

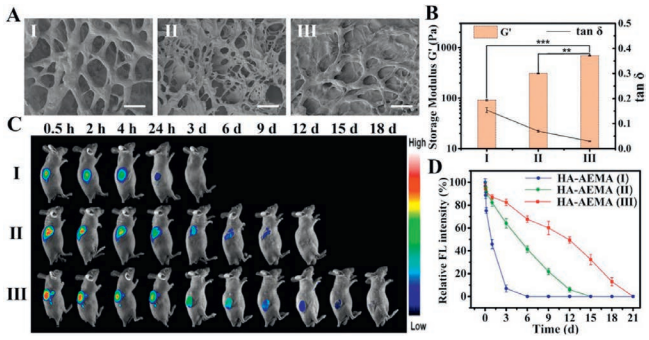


Fig. 3. Characterization of photopolymerized HA-AEMA hydrogel with variable 808 nm laser durations: HA-AEMA (I) for 5 min, HA-AEMA (II) for 7 min, and HA-AEMA (III) for 10 min. (A) SEM images. Scale bar: 100 μm. (B) Rheological characterizations. (C) *In vivo* fluorescence (FL) imaging of BALB/c Nude mice after receiving UCNPs/HA-AEME hydrogel of different cross-linking densities. (D) Relative FL intensity curve over time. Data are presented as mean ± standard deviation (SD) ($n = 3$). Statistical comparisons between two groups were conducted using one-way analysis of variance (ANOVA). $^{**}P < 0.01$, $^{***}P < 0.001$.

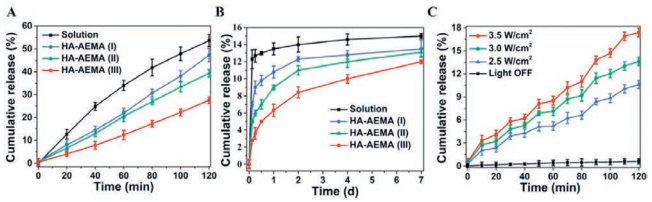


Fig. 4. *In vitro* cumulative release of 5-Fu triggered by 980 nm laser: (A) release profiles from the solution, hydrogels HA-AEMA (I), HA-AEMA (II) and HA-AEMA (III) under continuous 980 nm laser irradiation for 0–120 min. (B) release profiles of the solution and hydrogels HA-AEMA (I), HA-AEMA (II) and HA-AEMA (III) after an initial 20 min 980 nm laser irradiation, followed by no further laser exposure, and then the drug release was monitored over 7 days. (C) Release profiles from hydrogels HA-AEMA (III) under alternating "ON–OFF" laser excitation at varying power densities. Data are presented as mean ± SD ($n = 3$). Statistical comparisons between two groups were conducted using one-way ANOVA.

4, comprised 10 % (w/v) HA-AEMA, 2 % (v/v) NVP, 0.01 % (w/v) Eosin Y, 1 % (v/v) TEOA and 0.4 % (w/v) UCNPs. This mixture was exposed to an 808 nm NIR laser (3.5 W/cm^2) for variable durations (5, 7, and 10 min) to produce hydrogels named HA-AEMA (I), HA-AEMA (II) and HA-AEMA (III), respectively, with different cross-linking densities.

The morphology of the three hydrogels was characterized using scanning electron microscope (SEM) (Fig. 3A). SEM revealed that HA-AEMA (I) exhibited large and fluffy pores; HA-AEMA (II) displayed medium-sized pores with a less fluffy texture; and HA-AEMA (III) had the most compact structure. Using a Flory-Rehner model, we determined the effective cross-link densities (ν_e) and mesh sizes (ε) of UCNPs/HA-AEMA hydrogels (Table S3 in Supporting information). These findings indicate enhancements in cross-link densities and reductions in mesh sizes with increasing irradiation duration, consistent with SEM observations. Rheological assessments revealed storage moduli (G') of 91.0, 306.8 and 690.0 Pa for HA-AEMA (I), (II) and (III) hydrogels, respectively. Furthermore, the loss angle tangent (tan δ) values were calculated as 0.154, 0.070 and 0.030 by G"/G' accordingly (Fig. 3B and Fig. S4 in Supporting information), highlighting the strengthening effect of 808 nm irradiation on the hydrogel network. These results suggest that hydrogel density can be controlled *in-situ* using NIR light by adjusting the irradiation time.

To evaluate the hydrogels' stability *in vivo*, further imaging experiments were conducted on UCNPs/HA-AEMA hydrogels that were photopolymerized under 808 nm irradiation after subcutaneous injection. All animal procedures were performed in accordance with the Guidelines for the Care and Use of Laboratory Animals established by China Pharmaceutical University and approved by its Animal Ethics Committee (Approve No. 2024–07–139). As shown in Fig. 3C, the fluorescence signals of Eosin Y within the HA-AEMA (III) group exhibited prolonged retention. Quantitative analysis showed that the fluorescence signals in the HA-AEMA (III) group decreased much slower than those in the HA-AEMA (I) group, indicating that the former remained in the body for approximately 18 days until complete clean up (Fig. 3D). Without prior 808 nm irradiation, as shown in Fig. S5 (Supporting information), the composite exhibited significantly shorter retention (24 h) compared to groups subjected to 808 nm irradiation (HA-AEMA (I): 3 days, HA-AEMA (II): 12 days, and HA-AEMA (III): 18 days). These findings highlight the critical role of 808 nm irradiation in facilitating *in-situ* hydrogelation and achieving prolonged retention, which is essential for sustained therapeutic efficacy. These findings suggest that the *in vivo* stability of UCNPs/HA-AEMA hydrogels can also be adjusted by controlling the 808 nm NIR irradiation durations.

The synthesis and characterization of ONB-5-FU [39] are shown in Figs. S6–S11 and Table S4 (Supporting information). The light-triggered release of 5-FU from UCNPs/ONB-5-FU solution was first tested using UV light (Fig. S12 in Supporting information). The release rate was initially rapid but then gradually slowed down. After 2 h, drug release reached a plateau with a cumulative release of 89.0 %. Similarly, the solution was exposed to a 980 nm laser (3.5 W/cm^2), as shown in Fig. 4A (solution). The release trend was similar to that observed under UV light, while the release rate was relatively more stable. This suggests that the 980 nm photons were successfully upconverted to UV photons by the UCNPs, facilitating the activation of prodrugs. After 2 h of 980 nm excitation, the released drug was 53.6 %.

Next, we examined the activation release profiles of 5-FU from UCNPs/HA-AEMA/ONB-5-FU hydrogels with varying cross-linking densities. Under physiological conditions (pH 7.4, 37 °C) and continuous 980 nm irradiation, the release of 5-FU increased over time, demonstrating a near-linear relationship between the cumulative release amount and the duration of irradiation. Hydrogels with varying cross-linking densities displayed different 5-FU release rates. Hydrogels with higher cross-linking densities (HA-AEMA (III)) have smaller pore sizes, leading to slower release rates. Specifically, hydrogels with high cross-linking densities released only 27.5 % of drug over 2 h, in contrast to the 47.2 % released by low cross-linking hydrogels (HA-AEMA (I)), as shown in Fig. 4A. After 980 nm irradiation for 20 min, the release rates continued to differ significantly. High cross-linking hydrogels (HA-AEMA (III)) demonstrated a slow and sustained release, with only 6.3 % of 5-FU released after 1 day and 12.0 % after 7 days. In comparison, the low cross-linking hydrogels (HA-AEMA (I) and (II)) released 10.8 % and 13.5 % of the drug over the same periods, respectively, as illustrated in Fig. 4B The differences in release rates can be attributed to the variations in cross-linking densities and pore sizes between the hydrogels (Table S3 and Fig. 3A).

We also examined the effect of varying 980 nm laser power densities (2.5, 3.0, 3.5 W/cm^2) on the activation of ONB-5-FU from hydrogels using periodic ON/OFF cycles. The results showed that the drug release rate increased when the laser was “ON” and slowed when it was “OFF” (Fig. 4C). This release pattern remained consistent across all tested power densities, with higher power densities have faster release rates. Quantitative analysis revealed that the slope of the release curve during the “ON” phases was 3–5 times steeper than during the “OFF” phases. Notably, after 2 hours of irradiation at the highest power density of 3.5 W/cm^2, the cumulative release of 5-FU reached 17.4 %, significantly higher than the 0.6 % observed in hydrogels not subjected to laser activation.

These results highlight the capability of dual-wavelength orthogonal hydrogel system for facilitating on-demand drug release.

We next evaluated the anticancer efficacy of the dual-wavelength orthogonal UCNPs/ONB-5-FU hydrogel *in vitro* using the B16-F10 mouse malignant melanoma cell line. Initially, we assessed the cytotoxicity of both ONB-5-FU and 5-FU with a standard MTT assay. As depicted in Fig. S13 (Supporting information), ONB-5-FU exhibited minimal cytotoxicity to B16-F10 cells, suggesting high biocompatibility. In contrast, 5-FU demonstrated significant inhibition of B16-F10 cell proliferation at concentrations exceeding 5 μmol/L. The half maximal inhibitory concentration (IC_{50}) value for 5-FU in B16-F10 cells was determined to be 2.87 μmol/L.

Subsequently, we tested the viability of B16-F10 cells treated with UCNPs/ONB-5-FU in darkness or under 980 nm laser irradiation (2.5 W/cm^2, 50 s). As shown in Fig. S14 (Supporting information), UCNPs/ONB-5-FU alone demonstrated negligible cytotoxicity, confirming biosafety. Under 980 nm irradiation, however, cell viability decreased in a dose-dependent manner (2.5–10 μmol/L ONB-5-FU and 50–200 μg/mL UCNPs), with an IC_{50} of 7.49 μmol/L. Varying irradiation time (0–50 s, 2.5 W/cm^2) showed negligible cytotoxicity in the blank control but a marked, time-dependent reduction in viability when cells were treated with UCNPs/ONB-5-FU, especially beyond 40 s (Fig. S15 in Supporting information). When the irradiation power was increased to 3.5 W/cm^2 for 50 s (Fig. S16 in Supporting information), which was consistent with subsequent *in vivo* settings, only the UCNPs/ONB-5-FU group exhibited a marked therapeutic effect, indicating that our nanoplatform exhibits excellent biocompatibility.

To further understand the mechanism behind the observed cytotoxicity, we evaluated reactive oxygen species (ROS) generation in B16-F10 cells under different treatment conditions. We found that ROS levels were significantly elevated in B16-F10 cells treated with UCNPs/ONB-5-FU under 980 nm irradiation (Figs. S17 and S18 in Supporting information), indicating that the combination of UCNPs/ONB-5-FU and laser irradiation effectively induces ROS-mediated cytotoxicity. Similar results were observed in Live/Dead cell staining assays, where the UCNPs/ONB-5-FU group under 980 nm irradiation exhibited the highest cell death rate (98.99 %), significantly surpassing all other treatment groups (Figs. S19 and S20 in Supporting information). These results collectively confirm the effectiveness of light-controlled cytotoxicity in UCNPs/ONB-5-FU. To visualize the uptake of HA-modified water-soluble UCNPs by cells, the upconversion emission was observed using a BX53 Olympus fluorescence microscope. As shown in Fig. S21 (Supporting information), co-incubation with UCNPs resulted in a strong upconversion signal in B16-F10 cells, indicating effective uptake *via* CD44 receptors. Conversely, HaCaT cells showed a weaker signal due to fewer CD44 receptors. Pre-incubating B16-F10 cells with free HA (10 mg/mL) reduced UCNP uptake, confirming the role of CD44 receptors in targeting UCNPs.

Before conducting therapeutic experiments, we carefully monitored the temperature changes on mice under the laser irradiation. As shown in Figs. S22–S25 (Supporting information), the local temperature exposed to 808 and 980 nm increased to 30.1 and 30.2 °C, respectively, indicating a safe and controlled temperature rise with minimal overheating. In our study utilizing a B16-F10 xenografted tumor model in mice, we investigated the *in vivo* anticancer efficacy of the dual-wavelength orthogonal UCNPs/HA-AEMA/ONB-5-FU hydrogel, as illustrated in Fig. 5. We divided the treatment groups as follows: the phosphate buffered saline (PBS) control group (group a); tumors only treated with UCNPs/HA-AEMA hydrogel (group b); tumors treated with ONB-5-FU solution and 808 nm irradiation followed by 980 nm laser irradiation (group c); tumors treated with UCNPs/HA-AEMA/ONB-5-FU hydrogel without laser exposure (group d); and tumors treated with UCNPs/HA-AEMA/ONB-5-FU hydrogel along with 808 nm irradiation followed by 980 nm laser irradiation (group e). The results showed that groups b, c, and d exhibited moderate tumor growth rates without significant differences compared to the PBS control group. However, a notable distinction was observed in group e, where the UCNPs/HA-AEMA/ONB-5-FU hydrogel was applied in conjunction with 980 nm laser irradiation at 3.5 W/cm^2 for 50 s, markedly suppressed tumor growth (Figs. 5A, C and D). By day 15, the average tumor volume in group e was significantly reduced, showing a profound decrease compared to the PBS control group, with a statistical significance ($P < 0.001$).

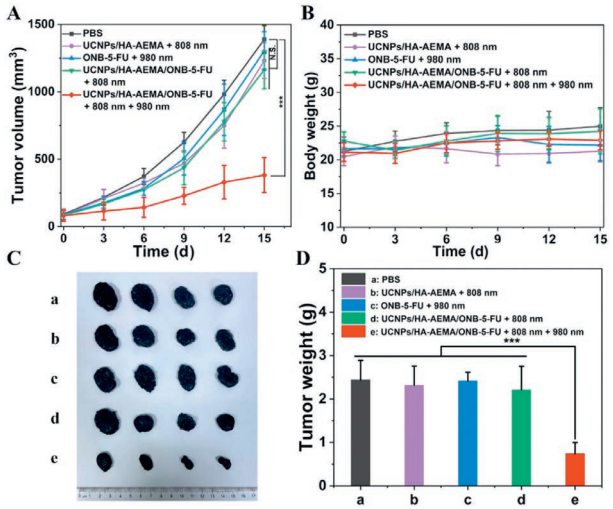


Fig. 5. Effect of *in vivo* treatment on changes in (A) tumor volume, (B) body weight, (C) optical images of tumor and (D) the tumor weight in BALB/c Nude mice. Data are presented as mean ± SD ($n = 4$). Statistical comparisons between two groups were conducted using one-way ANOVA. N.S., not significant. $^{***}P < 0.001$.

Further histological analyses of tumor tissues using hematoxylin and eosin (H&E) and terminal deoxynucleotidyl transferase dUTP nick end labeling (TUNEL) staining methods revealed treatment efficacy of the UCNPs/HA-AEMA/ONB-5-FU hydrogel. H&E staining showed that tumor tissues of group e, treated with UCNPs/HA-AEMA/ONB-5-FU hydrogel and 980 nm laser irradiation, exhibited the lowest cell density and extensive necrotic regions (Fig. S26E in Supporting information). In contrast, tumor cells in the PBS and other control groups (b, c, d) tumor cells were densely packed. TUNEL staining identified a significant quantity of apoptotic cells in group e, in contrast with the minimal apoptotic cells observed in the PBS group (Fig. S27 in Supporting information). These findings collectively suggest the UCNPs/HA-AEMA/ONB-5-FU hydrogel's effectiveness in cancer treatment when used together with 980 nm laser irradiation.

Additionally, we evaluated the systemic toxicity of the UCNPs/HA-AEMA/ONB-5-FU hydrogel after the treatment. H&E staining were employed to evaluate morphological alterations in the skin at the injection site and in major organs, including the heart, liver, spleen, lungs, and kidneys. Our findings, illustrated in Figs. S28 and S29 (Supporting information), revealed no significant morphological differences between the PBS group (group a) and the group treated with the hydrogel and dual-wavelength laser irradiation (group e) in all tissues assessed. Moreover, throughout the treatment period, all experimental groups, including the treated groups, demonstrated stable body weights, as shown in Fig. 5B. These results indicate the high biocompatibility of the UCNPs/HA-AEMA/ONB-5-FU hydrogel, highlighting its potential as a non-toxic treatment option for targeted cancer therapy.

In conclusion, the dual-wavelength orthogonal upconversion hydrogel nanoplatform demonstrates the feasibility of orthogonally triggering hydrogelation and drug release using dual-wavelength

NIR light. Utilizing well-engineered UCNPs, this system overcomes the limited penetration depths and spectral crosstalk that typically constrain traditional light-responsive hydrogels. The dual-wavelength functionality is crucial, with 808 nm NIR light excitation employed for *in-situ* hydrogel polymerization and 980 nm excitation for precise drug release. The successful encapsulation and targeted release of 5-FU within a HA-AEMA hydrogel matrix demonstrates its effectiveness in enhancing chemotherapy efficacy while minimizing systemic toxicity. We believe this versatile drug delivery system holds great potential to significantly improve cancer therapeutic outcomes in near future.

Declaration of competing interest

The authors declare that they have no known competing financial interests or personal relationships that could have appeared to influence the work reported in this paper.

CRediT authorship contribution statement

Minfei Yu: Writing – original draft, Methodology. **Yueyan Yang:** Methodology. **Xin Cheng:** Methodology. **Shicheng Pei:** Methodology. **Man Wu:** Methodology. **Fangling Cao:** Methodology. **Yaxin Zheng:** Methodology. **Shuyao Zhou:** Methodology. **Keming Xu:** Writing – review & editing, Supervision, Conceptualization. **Lei Zhou:** Writing – review & editing, Supervision, Methodology, Funding acquisition, Conceptualization. **Wenying Zhong:** Supervision, Funding acquisition.

Acknowledgments

This work was supported by National Natural Science Foundation of China (Nos. 62205379, 32471429, 82372114) and the Start-up Fund of China Pharmaceutical University (No. 3150050054).

Supplementary materials

Supplementary material associated with this article can be found, in the online version, at doi:10.1016/j.cclet.2025.111284.

References

[1] J. Li, D.J. Mooney, Nat. Rev. Mater. 1 (2016) 16071.
[2] Z. Zhao, Z. Wang, G. Li, et al., Adv. Funct. Mater. 31 (2021) 2103339.
[3] B.R. Freedman, A. Kuttler, N. Beckmann, et al., Nat. Biomed. Eng. 6 (2022) 1167–1179.
[4] C. Wu, C. Wang, Y. Zheng, et al., Adv. Funct. Mater. 31 (2021) 2104418.
[5] K. Zhang, Y. Zhou, J. Zhang, et al., Nat. Commun. 15 (2024) 249.
[6] F.G. Downs, D.J. Lunn, M.J. Booth, et al., Nat. Chem. 12 (2020) 363–371.
[7] H.F. Darge, E.Y. Hanurry, Y.S. Birhan, et al., Chem. Eng. J. 406 (2021) 126879.
[8] Y. Yan, J. Song, D. Liu, et al., Chin. Chem. Lett. 35 (2024) 109736.
[9] H. Ding, P. Tan, S. Fu, et al., J. Control. Release 348 (2022) 206–238.
[10] Z. Han, P. Wang, G. Mao, et al., ACS Appl. Mater. Interfaces 12 (2020) 12010–12017.
[11] J. Kang, X. Yang, X. Yang, et al., Chin. Chem. Lett. 35 (2024) 109297.
[12] M. Jain, G. Trapani, B. Trappmann, et al., Angew. Chem. Int. Ed. 63 (2024) e202403760.
[13] X. Wei, Y. Xue, Y. Sun, et al., Chem. Eng. J. 452 (2023) 139373.
[14] S. Wei, W. Lu, H. Shi, et al., Adv. Mater. 35 (2023) 2300615.
[15] Z. Jiang, M.L. Tan, M. Taheri, et al., Angew. Chem. Int. Ed. 59 (2020) 7049–7056.
[16] D. Wu, Z. Zhang, X. Li, et al., Acta Biomater. 168 (2023) 565–579.
[17] Y. Feng, Z. Zhang, W. Tang, et al., Exploration 3 (2023) 20220173.
[18] T. Song, H. Zhang, G. Liu, et al., View 5 (2024) 20230048.
[19] X. Guo, L. Li, W. Jia, et al., ACS Appl. Mater. Interfaces 16 (2023) 19926–19936.
[20] C. Zheng, F. Jin, Y. Zhao, et al., Sens. Actuators B: Chem. 304 (2020) 127345.
[21] M. Singh, J. Zhang, K. Bethel, et al., ACS Appl. Mater. Interfaces 13 (2021) 40365–40378.
[22] J.M. Scheiger, P.A. Levkin, Adv. Funct. Mater. 30 (2020) 1909800.
[23] Z. Yang, Y. Zhu, Z. Dong, et al., Biomaterials 281 (2022) 121332.
[24] M. Sitti, D.S. Wiersma, Adv. Mater. 32 (2020) 1906766.
[25] T. Jiang, Y. Zhang, J. Jiang, et al., Small 20 (2024) 2308352.
[26] L. Chen, X. Wei, Y. Sun, et al., Chem. Eng. J. 446 (2022) 137072.
[27] S.L. Walden, P.H. Nguyen, H.K. Li, et al., Nat. Commun. 14 (2023) 8298.
[28] Q. Liu, W. Feng, T. Yang, et al., Nat. Protoc. 8 (2013) 2033–2044.
[29] Y. Jiang, P. Fu, Y. Liu, et al., Sci. Adv. 6 (2020) eabc3513.
[30] C. Schiattarella, S. Romano, L. Sirleto, et al., Nature 626 (2024) 765–771.
[31] Y. Shang, J. Zhou, Y. Cai, et al., Nat. Commun. 11 (2020) 6156.
[32] Z. Li, S. Lu, W. Liu, et al., Angew. Chem. Int. Ed. 60 (2021) 19201–19206.
[33] L. Zhou, R. Wang, C. Yao, et al., Nat. Commun. 6 (2015) 6938.
[34] A.R. Chowdhuri, D. Laha, S. Pal, et al., Dalton Trans. 45 (2016) 18120–18132.
[35] B. Huang, J. Fu, T. Sun, et al., Chin. Chem. Lett. (2025), doi:10.1016/j.cclet.2025.111159.
[36] H. Dong, L. Sun, W. Feng, et al., ACS Nano 11 (2017) 3289–3297.
[37] X. Liu, H. Chen, Y. Wang, et al., Nat. Commun. 12 (2021) 5662.
[38] X. Han, Z. Li, J. Sun, et al., J. Control. Release 197 (2015) 29–40.
[39] L.L. Fedoryshin, A.J. Tavares, E. Petryayeva, et al., ACS Appl. Mater. Interfaces 6 (2014) 13600–13606.